Clays and Clay Minerals, Vol. 45, No. 2, 261–273, 1997.

PROPERTIES OF GOETHITE AND JAROSITE PRECIPITATED FROM ACIDIC GROUNDWATER, DALARNA, SWEDEN

ROGER B. HERBERT, JR.†

Institute of Earth Sciences, Uppsala University,
Norbyvägen 18B, 75236 Uppsala, Sweden

Abstract—This study characterizes various chemical and mineralogical properties of goethite and jarosite from a mine drainage environment using chemical extraction techniques, X-ray diffractometry (XRD), ^{57}Fe Mössbauer spectroscopy and scanning electron microscopy (SEM). Goethite and jarosite precipitates were collected from leachate-contaminated soils and from groundwater samples that were stored for up to 3 y. The results indicate that the soil goethites have primarily microcrystalline morphologies with moderately large mean crystallite dimensions ($MCD_{110} \sim 40$ nm), and are superparamagnetic at room temperature and magnetically ordered at 77 K. The substitution of Al for Fe in the goethites is less than 0.03 mol/mol, and there is consequently no measured contraction in the goethite unit cell volume. The jarosite unit cell dimensions, Mössbauer parameters and chemical compositions indicate that the precipitates are primarily well-crystallized K-Na-H_3O solid solutions, although the presence of poorly crystalline H_3O-rich jarosite is also identified in one sample.

Key Words—Acid Mine Drainage, Goethite, Groundwater, Jarosite, Mössbauer Spectroscopy, X-ray Diffractometry.

INTRODUCTION

The combined atmospheric oxidation of iron sulfides in mine waste deposits and the infiltration of water into the deposits generates an acidic, ferrous sulfate leachate in the pore solution. In unsaturated waste dumps overlying a shallow water table, the leachate will percolate through the deposit and the underlying soils and subsequently discharge to the groundwater. During the transport of the oxidation products in solution, Fe^{2+} commonly precipitates as hydrated ferrous sulfate efflorescences, or upon oxidation to Fe^{3+} as ferric oxyhydroxides or basic ferric sulfates (Nordstrom 1982). A variety of secondary Fe minerals have been identified in mine deposits and mine drainage systems, ranging in crystallinity from poorly ordered precipitates (such as ferrihydrite and schwertmannite) to more well-crystalline products (such as goethite and lepidocrocite); jarosite is the most commonly identified basic iron sulfate (Bigham 1994).

The chemistry and mineralogy of secondary Fe precipitates have been investigated in many acid mine drainage studies (Johnson 1986; Filipek et al. 1987; Karlsson et al. 1988; Blowes and Jambor 1990; Ficklin et al. 1991; Jambor 1994; Stollenwerk 1994; Ribet et al. 1995), but few of these studies have provided detailed analyses of precipitate crystallinity and morphology (Chapman et al. 1983; Brady et al. 1986; Alpers et al. 1989; Bigham et al. 1990; Bigham et al. 1994). However, these mineralogical studies have focused on precipitates forming in contaminated surface waters; none of the studies deals with the formation of precipitates from groundwater. As there seems to be less published data on Fe precipitates in this formation environment, the purpose of this study is to characterize the composition, morphology and crystallinity of secondary Fe minerals, particularly goethite and jarosite, precipitated from groundwater contaminated by mine leachate. These precipitates are investigated using chemical extraction techniques, SEM, XRD and ^{57}Fe Mössbauer spectroscopy.

MATERIALS AND METHODS

Field Site and Sampling

The samples discussed in this study were collected at a field site in the province of Dalarna, Sweden. The site consists of an abandoned Ni mine (Rudolfsgruvan) and a nearby rock dump containing sulfidic rock waste from the excavation of the mine. The rock dump is 2–3 m in thickness, covers a surface area of about 1500 m^2 and lies on glacial till that ranges in thickness from 2 to 5 m across the site. The underlying bedrock is granitic gneiss. The glacial till has developed from the gneissic bedrock, and it is consequently noncalcareous with a low acid neutralization capacity. Groundwater occurs in the unconfined till unit, and has been investigated in geochemical studies by Herbert (1994, 1995b). The studies indicate that the atmospheric oxidation of primarily pyrite (FeS_2) and pyrrhotite (Fe_7S_8), along with the percolation of water through the unsaturated rock dump, has led to the contamination of the groundwater. The groundwater chemistry directly down-gradient from the rock dump (well B1; Figure 1) is presented in Table 1.

To determine whether secondary Fe minerals were precipitating from the contaminated groundwater

† Email address: Roger.Herbert@geo.uu.se

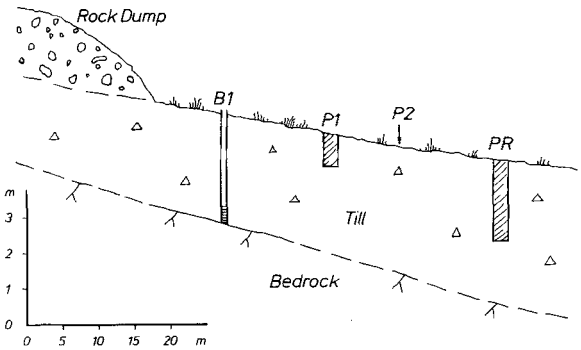

Figure 1. Cross section of field site showing sampling locations. B1 is a groundwater well and PR is a sampling pit. Pit P1 does not intercept the water table and is not mentioned in this study. Pit P2 is not located in the plane of the cross section.

down-gradient from the rock dump, 2 pits (P2, PR) were excavated in the till deposits to a depth that intersected the water table. Figure 1 illustrates the location of these pits in relation to the rock dump and the nearest well, B1. The soils from pits P2 and PR are podzols that have developed from sandy-silty glacial till. The soils have distinct accumulation (B) horizons approximately 20 to 50 cm below the ground surface. As the excavation of pit PR reached the water table (approximately 2.2 m depth; C horizon), a reddish-brown horizon of Fe oxide precipitation was observed; deeper excavation was not possible because of the hardness of the precipitate layer. The Fe oxide precipitates in PR appear very dark reddish-brown in color, occurring as massive coatings on mineral grains and as a cement, binding mineral grains and small pebbles together. Although Fe oxide mottling was observed at the base of pit P2 (2.2 m depth), the precipitation was much less extensive than observed in pit PR.

Soil samples were collected from the capillary fringe near the base of pit PR, no more than 0.2 m above the water table. These samples consisted of 1) fine-grained soils (<2 mm), and 2) conglomerates of Fe oxides, small pebbles and soil grains. After collection, the samples were dried at room temperature and then sieved to a grain size less than 63 μm; the fraction <4 μm was extracted by sedimentation in a water column. Following sedimentation, the samples were dried at 80 °C to remove excess water. Air-dried Fe oxide precipitate samples were removed by hand from the bulk of the sample matrix and pulverized in an agate mortar prior to analysis.

In addition to the soil and precipitate samples collected from the bottom of pit PR, precipitates were collected from groundwater samples. These were acquired 1) by filtering groundwater samples from well B1 in the field, and also 2) by allowing precipitates to form in groundwater samples after periods of storage (Alpers et al. 1989). For the filtered samples, groundwater samples were vacuum-filtered through 0.45-μm membrane filters, whereupon the filter residue was dried at room temperature for analysis. This material represents soil that was disturbed from around the well screen during groundwater sampling. The precipitated samples were obtained by storing groundwater samples collected in October 1992 and October 1993. At the time of sampling, both groundwater samples appeared light orange-red in color but were visibly free of suspended matter, and were stored unfiltered and at room temperature (22 ± 2 °C) for 2 to 3 y. During storage, it was noted that precipitates began to form in the water samples, and in November 1994 the precipitates were separated from the solutions by centrifugation, then freeze-dried. The samples discussed in this study are listed in Table 2.

Analytical Methods

The mineralogical composition of the secondary Fe phases was determined by powder XRD analysis using Cu*K*α radiation and a Philips 1710 diffractometer equipped with a diffracted-beam graphite monochromator. Randomly oriented powder samples were step-scanned from 10 to 80 °2θ at increments of 0.01 °2θ with a 10-s counting time. Peaks on the digitized XRD patterns were fitted with Voigt shape functions using Igor Pro™ (WaveMetrics 1994). The 2θ scale was calibrated using powdered silicon metal as an external standard. Although Co*K*α radiation is better suited to the analysis of Fe oxides (Schwertmann and Cornell

Table 1. Groundwater composition from well B1, May to October 1995. Samples filtered (0.45 μm) and analyzed by inductively coupled plasma-atomic emission spectroscopy (ICP-AES) and ion chromatography (sulfate); pH and redox potential (E_h) measured in field. Description of sampling techniques and analyses given in Herbert (1995b); *n* = number of sampling episodes; concentrations given in m*M*.

	n	Mean	Range		*n*	Mean	Range
pH	8	2.36	2.11–2.56	Al	8	5.8	4.1–8.0
E_h (mV)	7	497	476–523	K	2	0.03	0.02–0.03
SO_4	8	71.0	39.6–135.3	Na	2	0.3	0.3–0.3
Fe	8	39.6	17.0–83.6	Ca	2	6.8	6.6–7.0
Cu	8	0.9	0.5–1.6	Mg	2	2.9	2.8–2.9
Zn	8	0.5	0.3–1.0				

Table 2. Description of samples used in this investigation.

Sample	Description	Color (Munsell)	Secondary Fe minerals
G8, G16, G29	Precipitate separated from soil matrix, pit PR	2.5YR 2/4	Gt†, Lp‡
J14	Soil sample <4 μm, pit PR	10YR 7/4	J§
J89, J99	Well B1 filter residue, July 1995 and Oct 1995	10YR 7/4	J§
1092	Precipitate formed in groundwater sample, collected Oct 1992	7.5YR 5/8	Gt†, J§
1093	Precipitate formed in groundwater sample, collected Oct 1993, with small amount yellow fibers	2.5Y 8/6	J§

Key: † Gt goethite, ‡ Lp lepidocrocite, § J jarosite.

1991), since Cu$K\alpha$ radiation is strongly absorbed by Fe oxides and a high background is produced due to fluorescence radiation, these problems would not produce errors in line positions. While the fluorescence is removed by the graphite monochromator, the decrease in X-ray intensity caused by the absorption of Cu$K\alpha$ radiation may produce less intense reflections and different peak ratios than published values generated with Co$K\alpha$ radiation.

According to the XRD analyses from previous mineralogical studies of the field site (Herbert 1995a, 1996), goethite (α-FeOOH), jarosite [$KFe_3(SO_4)_2(OH)_6$] and minor amounts of lepidocrocite (γ-FeOOH) are present as secondary Fe precipitates in pit PR. As only small concentrations of lepidocrocite were identified in these reports, this study focuses on the characterization of goethite and jarosite. For the determination of goethite and jarosite unit cell dimensions, powdered Si metal was added to samples as an internal standard, and accurate peak positions were measured relative to nearby silicon peaks using a curve-fitting procedure. Unit-cell edge lengths of goethite (orthorhombic unit cell) and jarosite (hexagonal unit cell) were determined from the corrected peak positions using a least-squares method. For goethite, the first 3 major reflections [(110), (130), (111)] and the (221) reflection were used for cell edge determination; these line positions could be accurately determined for all samples. Although the major (110), (130), and (111) reflections are usually used for determining unit-cell dimensions (Schulze 1984; Schwertmann et al. 1985; Schwertmann and Carlson 1994), additional peaks are often included in order to reduce the error of estimation (Schwertmann and Carlson 1994). For jarosite, 7 reflections [(101), (012), (113), (006), (107), (033), (220)] were chosen; a similar number of reflections have been used in other jarosite studies (Alpers et al. 1989, 1992). For goethite, peak widths corrected for instrumental line broadening were used to calculate the mean crystallite dimensions perpendicular to the 110 and 111 planes (MCD_{110}, MCD_{111}), using the Scherrer formula (Klug and Alexander 1974). Instrumental line broadening (Schulze 1984) was estimated as the full width at half maximum height ($FWHM_{hkl}$) of the powdered quartz (20–5 μm) (131) reflection. As the goethite $FWHM_{110}$ and $FWHM_{111}$ never exceeded 0.5 °2θ, no correction was applied for diffraction line shifts caused by small particle sizes.

Mössbauer spectra were collected at room and liquid nitrogen temperatures (about 295 K and 77 K) using a ^{57}Co/Rh source and iron foil for velocity calibration. Spectra at liquid nitrogen temperature (approximately 77 K) were obtained by cooling the absorber in a cryostat. The transmitted radiation was recorded with a proportional counter and stored in a multichannel analyzer with 512 channels. After data collection, the mirror halves of the spectra were folded and were fitted with Lorentzian peaks using a least-squares data-fitting procedure. Spectra centroid shifts were calculated relative to the centroid of the room-temperature spectrum of metallic iron. While it is recognized that asymmetrically broadened lines in magnetically ordered goethite are most realistically fitted with distributions of hyperfine fields (Murad 1982), this was not done in the present study because of the lack of a suitable curve-fitting routine. Instead, the spectra were fitted with only 1 discrete sextet, which is assumed to approximate an average hyperfine field in the goethite within some margin of error.

Scanning electron microscopy was conducted with a Philips XL30 SEM equipped with a Philips XL30 energy dispersive spectroscopy (EDS) system. Semiquantitative analyses were performed using a "ZAF" matrix correction and quantification method. Since the EDS analyses are considered unreliable for $K\alpha$ peak intensities that are less than twice the background intensity, analyses are only discussed for cases in which there was sufficient intensity.

In order to determine the substitution of Al for Fe in goethite, the Fe and Al content in goethite was determined by extracting samples G8, G16 and G29 with a sodium dithionite-citrate-acetic acid (DCA) solution (pH 4.8) at room temperature for 4 h (Postma 1993), preceded by an ammonium oxalate extraction (pH 3; Schwertmann 1964). The DCA treatment dissolves poorly- to well-crystallized Fe oxides, while the oxalate pretreatment only dissolves poorly ordered Fe oxides (such as ferrihydrite, $Fe_5HO_8{\cdot}4H_2O$) and also lepidocrocite in the samples (Schwertmann 1973). The ratio of oxalate-soluble Fe (Fe_O) to DCA-soluble Fe

https://doi.org/10.1346/CCMN.1997.0450214 Published online by Cambridge University Press

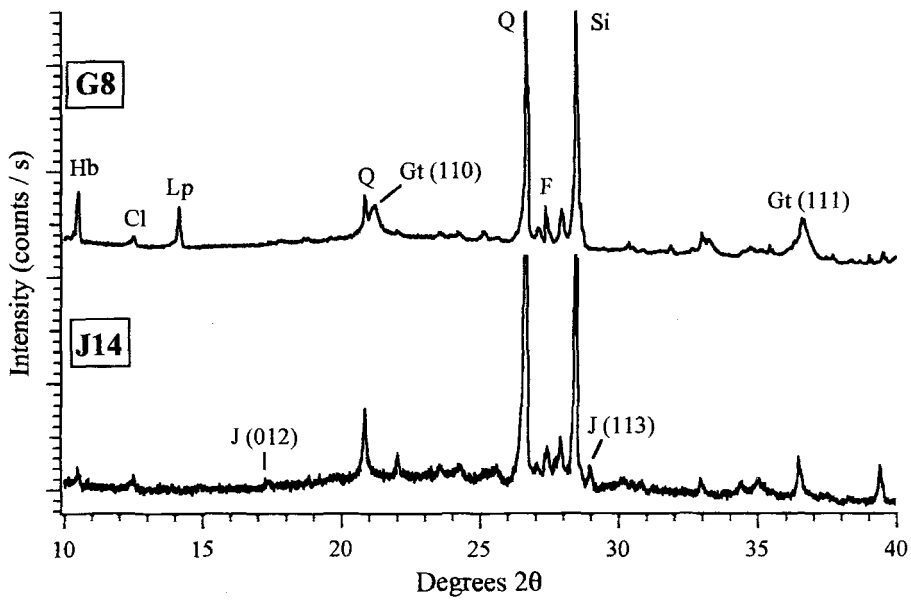

Figure 2. XRD pattern for G8 and J14. The peak positions are labeled with the *d*-values (Å). Key: Gt = goethite; Lp = lepidocrocite; Q = quartz; F = feldspar; Hb = hornblende; Si = silicon standard; Cl = chlorite. Major divisions on intensity scale equal 1000 counts/s.

(Fe_D) is 1 measure of the crystallinity of the precipitates; the Fe content extracted exclusively by DCA is represented as $Fe_{D\text{-}O}$. Analyses were performed by flame atomic absorption spectroscopy (AAS). The Al substitution in goethite was determined both from the amount of DCA-extractable Al ($Al_{D\text{-}O}$) relative to $Fe_{D\text{-}O}$ and from the *c*-axis length in the goethite unit cell. A relationship between Al substitution and the *c*-axis length has been derived by Schulze (1984) for a series of synthetic goethites, as Al (mol%) = 1730 − 572 *c*(Å). Later studies with natural goethites (Schwertmann et al. 1987; Schwertmann and Carlson 1994) indicated, however, that refined relationships were required for natural samples, since the cell dimensions of unsubstituted goethites were a function of the formation environment. The relationship used in this study Al (mol/mol) = 33.56 − 11.11 *c*(Å), is derived from a study of goethite formed at low temperatures as lake ores (Schwertmann and Carlson 1994). Total metal concentrations in selected samples were determined by dissolution in an aqua regia solution of concentrated HCl and HNO_3 (volume ratio 3:1). Iron, Al, Cu, Ni, Pb and Zn concentrations in the extracts were determined by flame AAS, while Na and K were determined by flame emission spectroscopy. Sulfate was determined by ion chromatography.

RESULTS

Mineralogical Composition

The minerals identified by XRD in samples G8, G16 and G29 are primarily goethite, quartz and feldspars with lesser amounts of lepidocrocite and hornblende (Table 2). The mineralogy of sample J14 consists primarily of quartz, hornblende and feldspars plus small amounts of mica (biotite), clay minerals (probably mixed-layer chlorite-vermiculite) and jarosite. With the exception of jarosite, the mineralogy of J14 is consistent with the fine silt fraction (<4 μm) of a Podzol C horizon developed from glacial till in this geographic location. The XRD patterns for G8 and J14 are shown in Figure 2, illustrating the relative abundances of the identified minerals.

Jarosite was the only secondary Fe mineral conclusively identifiable in the XRD pattern from samples J89, J99 and 1093 (Figure 3), while both jarosite and the broadened peaks ($WHH_{110} \approx 0.9$ °2θ) of a poorly crystalline goethite were identified in sample 1092 (Figure 3). These jarosites all have major peak positions and relative intensities typical of jarosite (JCPDS 1972, card 22-827). It should be noted that the broad peak centered around 22.2 °2θ (~4 Å), especially in sample 1093 (see Figure 3), is most likely produced by the glass slide used as a sample mount, and not from a poorly crystalline phase in the sample.

Precipitate Morphology and Chemical Composition

FE OXYHYDROXIDES. The SEM analysis of samples G8, G16 and G29 indicates that the Fe oxyhydroxides, consisting of goethite and lepidocrocite, generally have a microcrystalline morphology with no well-defined crystal habit. However, within void spaces where crystal growth is unhindered, more well-crystallized precipitates were identified, such as platey crystals approximately 2 to 5 μm in diameter (Figure 4a) as well

https://doi.org/10.1346/CCMN.1997.0450214 Published online by Cambridge University Press

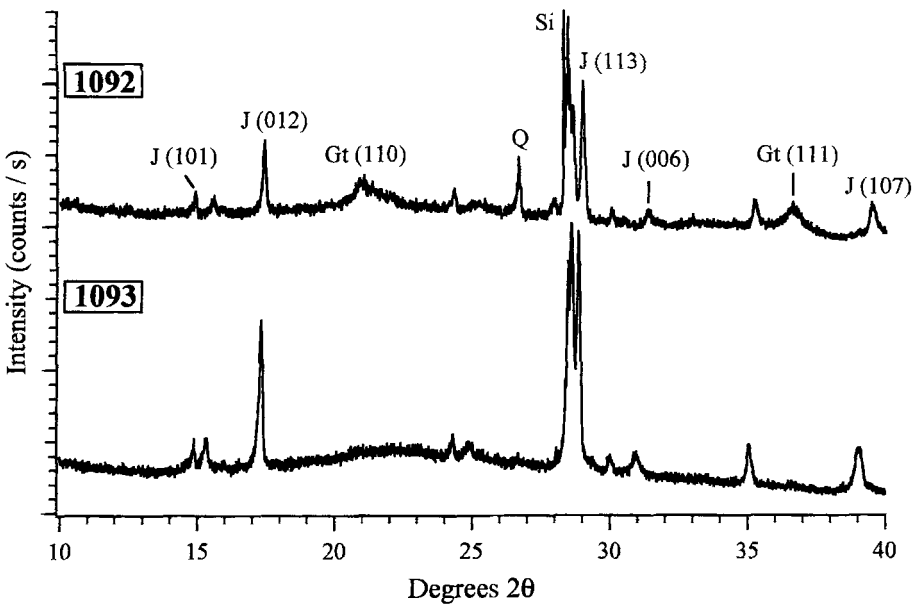

Figure 3. XRD pattern for 1092 and 1093. The peak positions are labeled with the *d*-values (Å). Key: Gt = goethite; J = jarosite; Si = silicon standard. Major divisions on intensity scale equal 1000 counts/s.

as aggregated spherical crystals about 0.5 to 2 μm in diameter (Figure 4b). The platey crystals may be lepidocrocite, which exhibit such a morphology when allowed to grow unhindered (Schwertmann and Taylor 1989). At higher magnifications (not shown), many bladelike acicular crystals smaller than 0.5 μm in length are revealed, radiating from the surfaces of the aggregated spherical crystals (Figure 4b), yielding a pincushion morphology. This morphology has been observed for schwertmannite (Bigham et al. 1994).

The results of the chemical extraction of samples G8, G16 and G29 are shown in Table 3. The samples have an Fe_O/Fe_D ratio of 0.18 to 0.28, indicating that a significant fraction of the Fe is soluble in oxalate, and that poorly crystalline goethite or Fe hydroxides (such as ferrihydrite or schwertmannite) may be present in these samples. Aluminum substitution values, determined chemically, are 0.01 to 0.03 mol/mol. Additional data on the heavy-metal content of these goethites and the isomorphous substitution of Al for Fe is presented in Herbert (1996).

JAROSITES. The jarosite family of compounds, $AFe_3(SO_4)_2(OH)_6$, consists of compounds where *A* is: H_3O^+, Na^+, K^+, Rb^+, Ag^+, NH_4^+, Tl^+, $½Pb^{2+}$ or $½Hg^{2+}$ (Dutrizac and Kaiman 1976), although most natural jarosites can be considered as solid solutions of jarosite [$KFe_3(SO_4)_2(OH)_6$], natrojarosite [$NaFe_3(SO_4)_2(OH)_6$] and hydronium jarosite [$H_3OFe_3(SO_4)_2(OH)_6$] (Brophy and Sheridan 1965). Jarosites are typically somewhat depleted in Fe (Dutrizac and Kaiman 1976), such that the Fe/S molar ratio is less than 1.5 (that is, 3 mol Fe:2 mol S). Ripmeester et al. (1986) demonstrated that, in such samples, in order to maintain charge neutrality, the Fe deficiency requires a conversion of OH^+ to H_2O in the jarosite structure.

The SEM analysis of 1092 shows that the sample is composed primarily of aggregates of pseudocubic crystals (<1 μm; Figure 4c). The EDS analyses detected distinct *K*α peaks for Fe, S, Al, K and Na, but the *K*α peak/background intensity ratio was greater than 2 for only the Fe, S and K peaks. The crystals possess an average Fe and S content of 36.2 and 13.9 wt%, respectively, yielding an Fe/S molar ratio of 1.50. These results indicate that these crystals are jarosite, exhibiting, on average, stoichiometric molar composition. The Fe/S ratio is much higher for interstitial precipitates, which bind together the jarosite aggregates (see Figure 4c); these have compositions similar to goethite with adsorbed sulfate (59.5 wt% Fe, 3.8 wt% S), but may also be ferrihydrite. Iron sulfate and Ca sulfate, probably as gypsum ($CaSO_4 \cdot 2H_2O$), are also detected by EDS (Figure 4c); however, considering that these sulfates do not occur intermixed with the jarosite crystals, but are rather draped over the top of the crystals, these probably formed during the deposition of this sample on the EDS stub prior to analysis.

After the recovery of sample 1093 from the sample bottle, a yellow precipitate was obtained along with a small amount of thin, yellow fibers. Subsequent analyses of these fibers by optical microscopy and SEM suggest that they are in fact fibers of polyethylene from the plastic bottle in which the sample was stored. The fibers were probably generated during the opening

https://doi.org/10.1346/CCMN.1997.0450214 Published online by Cambridge University Press

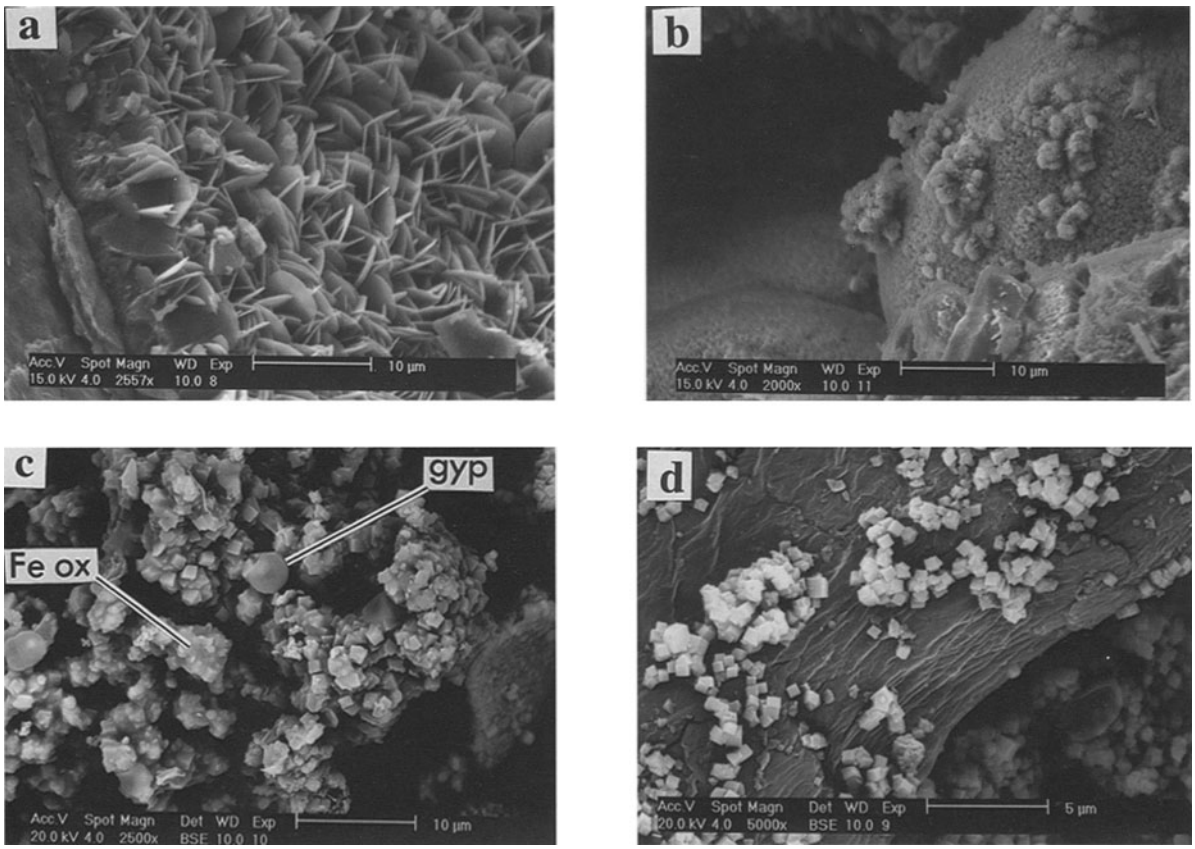

Figure 4. SEM back-scattered electron images of a) platey Fe oxyhydroxide crystals, sample G8; b) spherical Fe oxyhydroxide crystal aggregates with radiating acicular crystals, sample G8; c) pseudocubic jarosite crystals, sample 1092; and d) jarosite crystals on fiber, sample 1093. Note "gypsum" precipitates (gyp) draping over jarosite crystals in (4c) and presence of interstitial Fe oxide filling (Fe ox).

and closing of the bottle and/or during the collection of the precipitate from the bottle. As shown in Figure 4d, pseudocubic precipitates have formed in 1093 both on the polyethylene fibers and independently. These crystals are jarosite; the EDS analyses detected prominant Fe and S $K\alpha$ peaks with an average Fe/S molar ratio of 1.41; only minor K and Na peaks were observed. The EDS analysis of the fiber surfaces themselves, even when visually free of jarosite crystals at a scale down to at least 10 nm (Figure 4d), indicates that the surfaces have an elemental composition similar to jarosite (that is, EDS-detectable Fe, S and K $K\alpha$ peaks), although they are greatly depleted in Fe relative to S, with the Fe/S molar ratio ranging from 0.36 to 0.72. In addition, prominent carbon $K\alpha$ peaks are detected in these samples, although this should not be surprising, since polyethylene is an organic compound.

Since most of the samples analyzed in this study are complex mixtures of a number of mineral phases, the total chemical analysis of these samples would reveal little about the composition of individual mineral species. However, samples 1092 and 1093 contain only jarosite and Fe oxyhydroxides (see above). Therefore, the jarosite *A*-site compositions may be estimated from

Table 3. Properties of goethite precipitates. Numbers in parentheses are least-square standard errors; for example, (8) = ±0.008.

	Fe_O wt%	Fe_D wt%	$Al_{D,O}$ wt%	Fe_O/Fe_D	Unit-cell dimensions			Cell volume (Å^3)	Al (mol/mol)		MCD_{110} (nm)	MCD_{111} (nm)
					a (Å)	*b* (Å)	*c* (Å)		Chem†	XRD‡		
G8	5.58	19.83	0.18	0.28	4.611(1)	9.969(2)	3.023(1)	138.95	0.026	<0.0	52.1	41.8
G16	7.37	31.52	0.27	0.23	4.613(2)	9.984(6)	3.022(2)	139.18	0.023	<0.0	29.8	25.1
G29	5.30	29.80	0.20	0.18	4.610(3)	9.977(7)	3.022(2)	138.99	0.017	<0.0	46.5	21.2

† Chem: DCA extractable Al.
‡ XRD: Al (mol/mol) = 33.56 − 11.11 *c*(Å) (Schwertmann and Carlson 1994).

https://doi.org/10.1346/CCMN.1997.0450214 Published online by Cambridge University Press

Table 4. Chemical analyses of samples 1092 and 1093 and estimated jarosite stoichiometries. Fe, SO_4 and Al concentrations in units of wt%, all others in μg/g.

Sample	Fe	SO_4	Al	K	Na	H_3O	Cu	Ni	Pb	Zn
Chemical results										
1092	36.8	11.5	0.25	11077	7385	–	615	154	0	7154
1093	31.0	8.7	<0.01	2358	1504	–	1016	610	0	854
Molar composition										
1092	3.0	2.0	(0.08)	0.47	0.53	0.00	–	–	–	–
1093	2.8	2.0	–	0.13	0.14	0.73	–	–	–	–

the dissolution of jarosite/goethite mixtures, since most K and Na extracted from the samples can be expected to come only from jarosite. The results from the chemical extraction of samples 1092 and 1093 are shown on Table 4. If it is assumed that 2 mol SO_4 are present in the jarosite structure and the jarosite *A*-site consists of only K^+, Na^+ or H_3O^+ ions with a total of 1 mol per unit formula, then the jarosite composition may be calculated relative to the SO_4 total. Since the aqua regia extractions remove Fe from both jarosite and Fe oxides, the Fe/S molar ratio for these samples is far greater than 1.5. Therefore, the Fe/S molar ratio is taken from the EDS results. The low concentrations of Al detected in 1092 are ignored in these compositional calculations, since the Al content would be less than 0.1 mol per unit formula. A mean jarosite composition is calculated for 1092 as $(K_{0.47}Na_{0.53})Fe_{3.00}(SO_4)_2(OH)_6$ and for 1093 as $(K_{0.13}Na_{0.14}H_3O_{0.73})Fe_{2.81}(SO_4)_2(OH)_6$. Substantial levels of the heavy metals Cu, Ni, Pb and Zn are extracted from 1092 and 1093 (Table 4), and are probably coprecipitated with Fe oxyhydroxides present in the samples.

Although the jarosite precipitates have formed in a closed system, the chemical analysis of the solution composition before and after storage (data not shown) showed that the Fe, SO_4^{2-}, K and Na concentrations decreased by less than 10%. Similar findings were reported by Alpers et al. (1989). This suggests that the lack of ion replenishment to the solution, which occurs in open systems through mineral weathering, should not have affected the jarosite compositions, since the solution composition did not greatly change during storage.

Table 5. Unit-cell dimensions of jarosite precipitates. Numbers in parentheses are least-square standard errors; for example, (8) = ±0.008.

	Unit-cell dimensions		Cell volume
	a (Å)	*c* (Å)	Å^3
J14	7.301(6)	17.151(9)	791.73
J89	7.312(7)	17.121(13)	792.66
J99	7.310(8)	17.096(25)	791.15
1092	7.304(7)	17.104(11)	790.23
1093	7.303(5)	17.319(11)	799.86

Unit-Cell Dimensions

The properties of selected goethite samples determined by XRD are shown in Table 3, and indicate that the unit-cell dimensions and cell volumes are similar for G8, G16 and G29. The Al substitutions determined from the *c* dimensions are less than zero, but this is expected since the *c* dimension of unsubstituted goethites from Schwertmann and Carlson (1994) was estimated from regression analyses as 3.020 ± 0.002 Å. Although the XRD-determined Al substitutions and the chemically determined values differ somewhat, the differences are not great and are within 1 standard deviation (Schwertmann and Carlson 1994; ±0.022 mol/mol). Compared with a goethite cell volume corresponding to zero Al substitution (139.0 ± 0.2 Å^3; Schwertmann and Carlson 1994), samples G8, G16 and G29 exhibit no contraction in unit-cell volume. The MCD_{111} and MCD_{110} estimates for the goethites indicate moderately large crystal sizes.

The jarosite unit cell dimensions calculated from the XRD analyses are presented in Table 5. The results indicate that the *a* dimensions are approximately the same, coinciding within 1 standard deviation (~± 0.007 Å). The *c* dimensions, however, range from 17.096 Å (J99) to 17.319 Å (1093). The calculated jarosite unit cell volumes are similar, with the exception of sample 1093, which is much larger.

Mössbauer Spectroscopy

Samples G8, 1092, 1093 and J14 were analyzed by ^{57}Fe Mössbauer spectroscopy at room temperature and 77 K; the Mössbauer parameters of these samples are shown in Table 6. As shown in Figure 5, the room temperature spectrum for G8 consists of a weak Fe^{2+} doublet and a strong Fe^{3+} doublet with a strongly relaxed magnetically ordered component. The ferrous doublet corresponds to the hornblende M123 sites (Goldman 1979); absorption from the individual hornblende sites was too weak to be fitted. The ferric component is broad (FWHM = 0.67 mm/s) and is fitted with 2 doublets: one is assigned to superparamagnetic goethite or lepidocrocite (ΔE_Q = 0.56 mm/s), and the other with a greater quadrupole splitting (ΔE_Q = 0.87 mm/s) is assigned to a poorly ordered Fe oxyhydroxide (such as goethite, ferrihydrite or schwertmannite;

https://doi.org/10.1346/CCMN.1997.0450214 Published online by Cambridge University Press

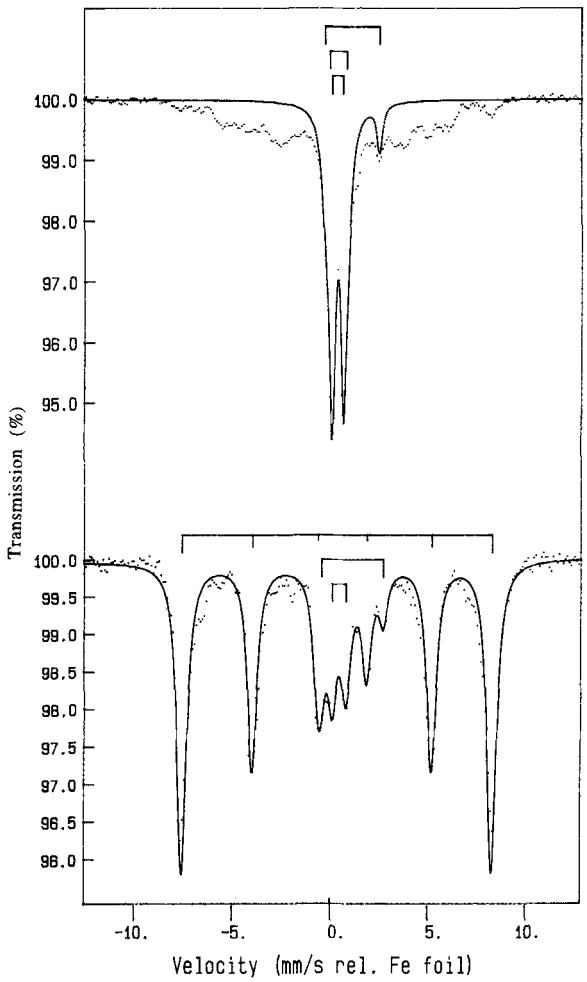

Figure 5. Mössbauer spectra for G8 at room temperature (above) and 77 K (below).

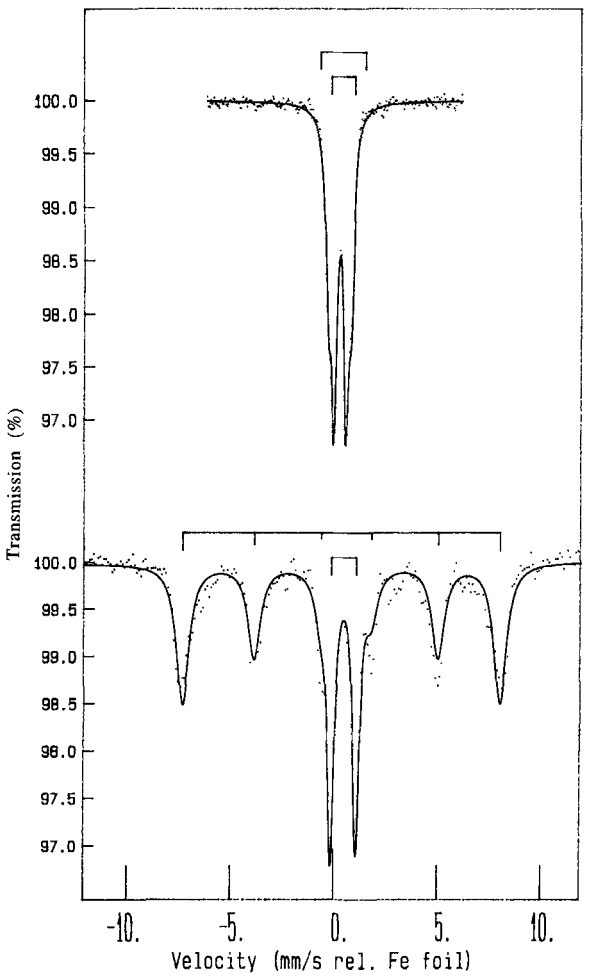

Figure 6. Mössbauer spectra for 1092 at room temperature (above) and 77 K (below).

Murad and Schwertmann 1980; Murad et al. 1990). At 77 K, a magnetically ordered component with fairly symmetric lines is observed along with a doublet (Figure 5); the paramagnetic doublet corresponds to lepidocrocite, but may also have contributions from a fraction of the goethite that is superparamagnetic at 77 K, or ferrihydrite. The magnetic component has been fitted with 1 sextet, where the hyperfine field (B = 49.2 T) and quadrupole splitting (ΔE_Q = −0.25 mm/s) are consistent for goethite, although the field is less than produced by the most well-crystalline goethites (50.3 T, Schwertmann and Taylor 1989). The fitted sextet in G8 (Figure 5) is symmetric and probably represents the hyperfine fields of a relatively narrow range of particle sizes.

The room-temperature spectrum for 1092 is fitted with 2 ferric absorption doublets (Figure 6): the outer doublet has a quadrupole splitting (ΔE_Q = 1.12 mm/s) typical of jarosites (ΔE_Q = 1.00 to 1.20 mm/s; Leclerc 1980), while the inner is fitted as a superparamagnetic ferric compound (ΔE_Q = 0.57 mm/s). At 77 K, jarosite is again present and an asymmetrical magnetically ordered component is resolved; it is fitted with 1 sextet (47.7 T), assigned to goethite. However, this asymmetrical sextet could also be fitted with a distribution of fields, where a significant fraction of the magnetically ordered component would probably be assigned a hyperfine field less than approximately 48 T. A distribution of hyperfine fields is usually derived from ^{57}Fe resonance in goethites having a range of particle sizes and hence with different magnetic characteristics (Schwertmann et al. 1985).

For sample 1093, the room-temperature spectrum is fitted with 3 doublets (Figure 7). The inner 2 doublets correspond to an Fe oxyhydroxide and jarosite (ΔE_Q = 0.54 mm/s and 1.01 mm/s, respectively). The outer doublet is fitted with a quadrupole splitting (ΔE_Q = 1.86 mm/s) that is unusually large for typical ferric compounds observed in acid mine drainage studies, and is difficult to assign to a common Fe precipitate.

https://doi.org/10.1346/CCMN.1997.0450214 Published online by Cambridge University Press

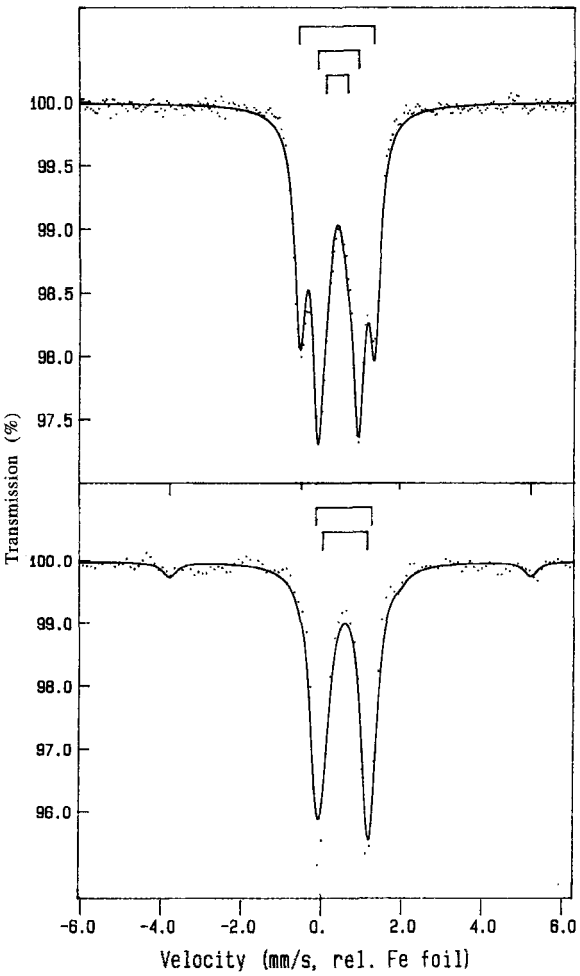

Figure 7. Mössbauer spectra for 1093 at room temperature (above) and 77 K (below). Note different scale; outer sextet peaks not shown for 77-K spectrum.

It is likely that this absorption peak is derived from ^{57}Fe associated with the surface of the polyethylene fibers in the sample. The spectrum at liquid nitrogen temperature is composed of a very weak magnetic component which can be attributed to goethite, and a central paramagetic doublet. The doublet consists of contributions from jarosite (ΔE_Q = 1.11 mm/s) and the unknown Fe compound.

The Mössbauer spectrum at room temperature of the soil sample from pit PR (J14) consists of an inner ferric doublet and a lesser outer ferrous doublet (spectrum not shown; Figure 6). The ferrous component corresponds to hornblende, and the inner peaks are fitted with 2 doublets: the outer ferric peaks (ΔE_Q = 1.10 mm/s) are assigned to jarosite, while the inner peaks (ΔE_Q = 0.58 mm/s) are contributions from Fe^{3+} oxyhydroxides. The 77-K spectrum for sample J14 possesses a magnetic component with asymmetric lines; this component is fitted with 1 sextet (48.3 T) corresponding to goethite.

Based on the fitted Mössbauer parameters for the samples (Table 6), it is not expected that any other mineral but goethite is magnetically ordered in these samples at 77 K. Lepidocrocite has a Néel temperature of 77 K (Murad 1988), and while the liquid nitrogen-cooled cryostats are nominally cooled to 77 K, the temperature is actually somewhat higher, so magnetic ordering in lepidocrocite at "77 K" is not expected. More poorly crystalline Fe oxides such as schwertmannite (Murad et al. 1990; Bigham et al. 1994) and ferrihydrite can exhibit partial magnetic-ordering at 77 K in better-crystallized samples (Murad 1988; Bigham 1994), but low concentrations of these components would be masked by the asymmetrical goethite sextets. It is possible that schwertmannite or ferrihydrite has precipitated at the water table, and their presence is

Table 6. Mössbauer parameters of selected samples at room temperature and at 77 K.

Sample	Room temperature			77 K				Probable mineral‡
	I	CS	ΔE_Q	I	CS†	ΔE_Q†	B†	
G8	0.11	1.11	2.78	0.06	1.12	3.17	–	Hb
	0.49	0.37	0.56	0.79	0.48	−0.25	49.2	Gt
	0.39	0.40	0.87	0.15	0.44	0.72	–	Lp/Fe^{III}min
J14	0.13	1.10	2.68	0.15	1.22	3.03	–	Hb
	0.21	0.39	1.10	0.28	0.49	1.16	–	J
	0.66	0.37	0.58	0.41	0.46	−0.29	48.3	Gt
				0.15	0.42	0.58	–	Fe^{III}min
1092	0.36	0.38	1.12	0.38	0.49	1.22	–	J
	0.64	0.38	0.57	0.62	0.48	−0.24	47.7	Gt
1093	0.50	0.39	1.01	0.50	0.51	1.11	–	J
	0.35	0.36	1.86	0.36	0.48	1.39	–	J
	0.15	0.39	0.54	0.14	0.54	−0.24	48.3	Gt

† CS = centroid shift relative to metallic Fe foil, mm/s; ΔE_Q = quadrupole splitting, mm/s; B = magnetic hyperfine field, tesla (T).

‡ Gt = goethite; Lp = lepidocrocite; J = jarosite; Hb = hornblende; Fe^{III}min = unidentified ferric minerals. "Probable mineral" refers to 77 K analysis.

https://doi.org/10.1346/CCMN.1997.0450214 Published online by Cambridge University Press

suggested by the relatively high Fe_O/Fe_D ratios for samples G8, G16 and G29, the SEM investigation and the persistence of a (super-)paramagnetic doublet at 77 K. However, poorly crystalline goethite and lepidocrocite also yield a rather high Fe_O/Fe_D ratio and lack magnetic order at 77 K; this investigation does not provide enough information to determine the concentrations of these various less-crystalline phases. Mössbauer measurements could be taken at lower temperatures to conclusively quantify the levels of these Fe species in the samples, and such techniques as differential X-ray diffractometry (Schulze 1981) could be used to complement such analyses.

DISCUSSION AND CONCLUSIONS

Goethite Crystallinity

The crystallinity of Fe oxyhydroxides is a function of the formation environment, which includes the rate of bacterially mediated Fe^{2+} oxidation and subsequent Fe^{3+} hydrolysis and precipitation, the solution pH and the presence of compounds that interfere with crystal nucleation and growth (for example, Si, Al, PO_4^{3-} and organic matter). Crystallinity is a term used to reflect crystal size and structural defects (Schwertmann 1985), and is often quantified by measuring the width of diffraction lines in XRD patterns and peak widths in Mössbauer spectra. The broadening of XRD lines reflects the average size and shape of the crystal, or more exactly, that of coherently scattered domains in the crystals (Schulze and Schwertmann 1984).

The Fe oxyhydroxides studied in samples G8, G16 and G29 have primarily microcrystalline morphologies, although well-crystallized Fe oxyhydroxides are observed in void spaces in the precipitates (Figures 4a and 4b). As shown in Figure 2, the major (110) and (111) peaks for goethite exhibit only moderate broadening ($FWHM_{110} \sim 0.3$ °2θ). The MCD_{111} and MCD_{110} estimates from these line broadenings (Table 3) indicate moderately large crystallite sizes (21–52 nm), which are larger than other published MCD values for low Al-substituted goethites (<0.05 mol/mol) from soils and aquatic environments (Campbell and Schwertmann 1984; Schwertmann 1985; Schwertmann et al. 1987).

Although pure, well-crystallized goethite is magnetically ordered below about 400 K (Murad 1988), goethite is rarely pure in nature and the substitution of Al for Fe in goethite and reduced crystallinity (small particle size) may yield a partial or complete breakdown of magnetic order at room temperature, resulting in the phenomenon of superparamagnetic relaxation. For superparamagnetic goethite, the blocking temperature exists below room temperature but at least partial magnetic order is usually observed at 77 K. The room-temperature Mössbauer analyses indicate that there is a partial breakdown in magnetic order in the moderately well-crystallized goethites (G8, Figure 5), and a complete collapse of the magnetic hyperfine field in more poorly crystalline samples (J14, 1092, 1093). Since the substitution of Al for Fe in the goethites is very low (0.01 to 0.03 mol/mol; Table 3), the partial or complete collapse of the magnetic hyperfine field at room temperature is probably the result of the small particle size/low crystallinity of the precipitates. The samples exhibit at least partial magnetic ordering at 77 K, while the greater hyperfine field measured in G8 relative to J14, 1092 and 1093 supports a greater goethite crystallinity in G8.

Previous mineral equilibria studies (Herbert 1994, 1995a, 1995b), using geochemical conditions observed near well B1 (Table 1), have concluded that goethite is the most stable secondary Fe mineral forming in the groundwater. Lepidocrocite reaches saturation in the groundwater only during snowmelt when groundwater pH increases (Herbert 1995b). The processes generally controlling lepidocrocite's stability relative to goethite are 1) the substitution of Al for Fe, 2) the rate of Fe^{2+} oxidation and 3) the presence of carbonate species (Schwertmann and Taylor 1989). At this field site, the low substitution of Al for Fe in goethite and the negligible carbonate level in the groundwater should not impede the formation of lepidocrocite. Therefore, the rate of Fe^{2+} oxidation probably determines the precipitation of goethite over lepidocrocite; a low rate of Fe^{2+} oxidation would favor goethite formation (Carlson and Schwertmann 1990). As particle size is a major control on the relative thermodynamic stabilities of Fe oxyhydroxides (Langmuir and Whittemore 1971), the large particle sizes of the goethite precipitates indicate that these precipitates should be stable in the groundwater at the current geochemical conditions.

Jarosite Composition

Brophy and Sheridan (1965) established that the jarosite hexagonal unit cell dimensions vary systematically but nonlinearly with changes in solid solution composition. The variation in *c* relative to *a* is related to the cation size and is controlled by the crystal structure (Brophy et al. 1962), where the *A*-site composition affects primarily the *c* edge length. As demonstrated in Figure 8 (Table 5), the *a* dimensions of samples J14, J89, J99 and 1092 are within about 1 standard deviation of the jarosite end-member *a* edge length, but the *c* dimensions deviate considerably (a = 7.29 Å, c = 17.16 Å; JCPDS 1972), indicating that these samples are not pure jarosites. These samples plot fairly closely to the imaginary line separating the K- and H_3O-jarosite end members, suggesting a primarily K-H_3O solid solution. However, if the jarosite is a multicomponent solid-solution series, XRD becomes unreliable as a unique means of identification,

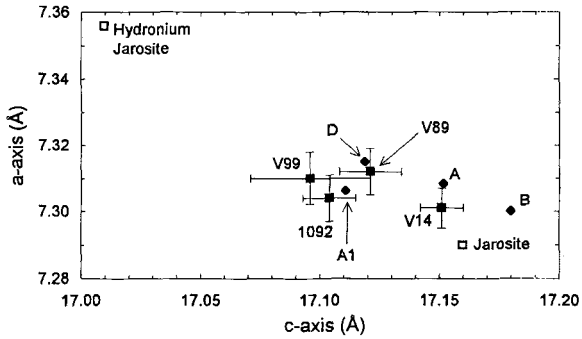

Figure 8. Relationship between *a* and *c* dimensions for investigated jarosites (closed squares) and other published values (closed diamonds). The end-member jarosite and hydronium jarosite dimensions (open squares) are taken from JCPDS files (1972) 22-827 and 21-932, respectively. Error bars show least-squares errors (Table 5). Key to other published values (closed diamonds): Sample A = $(K_{0.77}Na_{0.03}H_3O_{0.20})Fe_{3.00}(SO_4)_2(OH)_6$, Alpers et al. (1989); Sample A1 = $(K_{0.53}Na_{0.15}H_3O_{0.32})Fe_{3.00}(SO_4)_2(OH)_6$, Alpers et al. (1992); Sample D = $(K_{0.86}H_3O_{0.14})Fe_{2.49}(SO_4)_2(OH)_6$, Dutrizac and Kaiman (1976); Sample B = $(K_{0.47}Na_{0.02}H_3O_{0.51})Fe_{3.00}(SO_4)_2(OH)_6$, Brophy and Sheridan (1965).

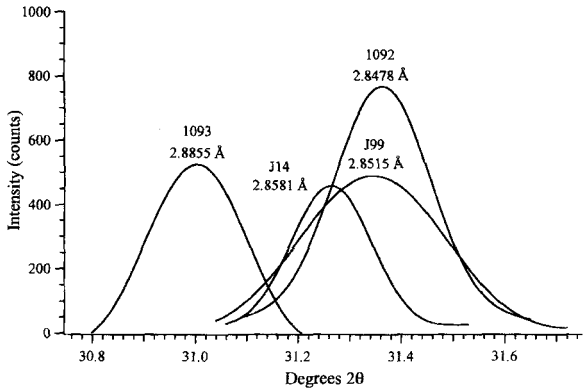

Figure 9. XRD diagram of jarosite (006) peaks for samples J14, J99, 1092 and 1093. Peaks fitted with Voigt functions, background removed. Peak positions corrected relative to position of nearest Si peak (Figures 2 and 3).

and should be combined with chemical analyses (Dutrizac and Kaiman 1976).

A comparison of jarosites from other investigations clearly demonstrates that there is a large variation in the composition of the K-Na-H_3O solid solutions at cell dimensions close to the K-rich end-member (Figure 8) (Brophy and Sheridan 1965; Dutrizac and Kaiman 1976; Alpers et al. 1989; Alpers et al. 1992). Similarly, the chemical extraction of samples 1092 and 1093 (Table 4) indicates that these samples are K-Na and K-Na-H_3O solid solutions, respectively, but with cell dimensions most like the K-rich end-member. It appears that only very high Na substitutions in the *A*-site will produce a jarosite with contracted *c* dimensions close to those published for natrojarosite (c = 16.72 Å; JCPDS 1972).

The Mössbauer parameters of the jarosites are difficult to interpret, since the potential Fe depletion in the jarosite structure and the *A*-site solid solution complicate the comparison of samples. As the onset of magnetic ordering in jarosites occurs around 60 K (Leclerc 1980), there are no data regarding the magnetic hyperfine field. However, the quadruple splittings (room temperature) for jarosite in J14 and 1092 are the range of Na- and K-rich jarosites (ΔE_Q = 1.05 – 1.13 mm/s; Leclerc 1980), which agrees with the chemical analyses for 1092; and the quadrupole splitting for the inner doublet in 1093 is close to the value for hydronium jarosite (1.00 mm/s; Leclerc 1980), also in agreement with the chemical analyses. The peak widths (mean FWHM = 0.33 mm/s) of the jarosite doublets indicate that these precipitates are well crystallized, as supported by the SEM analyses (Figures 4c and 4d).

The relatively low substitution of K^+ in the *A*-sites reflects the groundwater chemistry (Table 1), which contains very low concentrations of K (0.03 m*M*) relative to Na (0.3 m*M*; Herbert 1995b). This is attributable to the greater weatherability of hornblende and Na-plagioclase in the glacial till, relative to resistant K-feldspar. Although jarosite was undersaturated in all groundwater samples collected from B1 over the course of several years (Herbert 1995b), equilibrium with respect to the K-rich end member in the jarosite solid solution is probably unrealistic, considering the observation that the jarosites in this study are K-Na-H_3O solid solutions. Instead, saturation may be achieved with respect to a jarosite solid solution with a significant hydronium content; such findings have been reported previously (Alpers et al. 1989).

Sample 1093

According to the XRD analysis of sample 1093 (Table 5), this jarosite has an unusually large *c* dimension. Relative to the other samples, certain peak positions [(003), (006), (107) reflections] in sample 1093 are shifted to larger angles (greater *d*-spacings). The *c* estimates are quite sensitive to the position of the (006) peak; as shown in Figure 9, the (006) reflections for J14, J99 and 1092 are slightly less than the published *d*-spacing of 2.861 Å, while the reflection from 1093 is at a much larger spacing. The Mössbauer results also suggest that sample 1093 is unusual; the outer doublet is fitted with a quadrupole splitting (1.86 mm/s) which is very large for ferric compounds.

The unusual *c* axis dimensions and Mössbauer parameters for sample 1093 are probably related to the accidental contamination of this sample with polyethylene fibers from the sample bottle. Although the fibers themselves are not expected to affect the XRD or

Mössbauer analyses, these fibers have provided surfaces for the precipitation of jarosite in the sample bottle. The SEM-EDS analyses indicate that the composition of the fiber surface is similar to jarosite, but with a composition greatly depleted in Fe relative to S. This suggests that jarosite may be present on the fiber surface as crystals <10 nm in size. Thus, the large *c* dimension may not be due to a large unit cell but may in fact reflect a shift in jarosite line positions due to X-ray diffraction from very small particles (Brindley 1980). As noted by Schulze (1984) for small goethite particles, line shifts can occur if the Lorentz-polarization factor and/or the structure factor are not essentially constant over the angular range of a broad diffraction line. Similarly, the large ΔE_Q in 1093 may be derived ^{57}Fe resonance in poorly crystalline, Fe-depleted jarosite particles on the fibers. Leclerc (1980) observed that a reduction in Fe content from stoichiometry in jarosites coincided with an increase in ΔE_Q, suggesting that an increased depletion of Fe results in an increase in site distortion and a decrease in octahedral symmetry.

ACKNOWLEDGMENTS

I wish to thank H. Annersten, T. Eriksson and A. A. Aldahan for their useful comments. The remarks of 2 anonymous reviewers greatly improved the contents of this paper. The Mössbauer and SEM analyses were financed by a research grant from Stiftelsen Oscar och Lili Lamms Minne. Financial support has also been provided by Uppsala University and the Royal Swedish Academy of Sciences.

REFERENCES

Alpers CN, Nordstrom DK, Ball JW. 1989. Solubility of jarosite solid solutions precipitated from acid mine waters, Iron Mountain, California, USA. Sci Géol Bull 42:281–298.

Alpers CN, Rye RO, Nordstrom DK, White LD, King B-S. 1992. Chemical, crystallographic, and stable isotopic properties of alunite and jarosite from acid-hypersaline Australian lakes. Chem Geol 96:203–226.

Bigham, JM. 1994. Mineralogy of ochre deposits formed by sulfide oxidation. In: Jambor J, Blowes D, editors. Handbook on environmental geochemistry of sulfide minewastes. Mineral Assoc Can 22:103–132.

Bigham JM, Carlson L, Murad E. 1994. Schwertmannite, a new iron oxyhydroxy-sulphate from Pyhäsalmi, Finland, and other localities. Mineral Mag 58:641–648.

Bigham JM, Schwertmann U, Carlson L, Murad E. 1990. A poorly crystalline oxyhydroxysulfate of iron formed by bacterial oxidation of Fe(II) in acid mine water. Geochim Cosmochim Acta 54:2743–2758.

Blowes DW, Jambor JL. 1990. The pore-water chemistry and the mineralogy of the vadose zone of sulfide tailings, Waite Amulet, Quebec, Canada. Appl Geochem 5:327–346.

Brady KS, Bigham JM, Jaynes WF, Logan TJ. 1986. Influence of sulfate on Fe-oxide formation: Comparisons with a stream receiving acid mine drainage. Clays Clay Miner 34:266–274.

Brindley GW. 1980. Order-disorder in clay mineral structures. In: Brindley GW, Brown G, editors. Crystal structures of clay minerals and their X-ray identification. London: Mineral Soc. p 125–195.

Brophy GP, Scott ES, Snellgrove RA. 1962. Sulphate studies II. Solid solution between jarosite and alunite. Am Mineral 47:112–126.

Brophy GP, Sheridan FS. 1965. Sulphate studies IV: The jarosite-narojarosite-hydronium jarosite solid solution series. Am Mineral 50:1595–1607.

Campbell AS, Schwertmann U. 1984. Iron oxide mineralogy of placic horizons. J Soil Sci 35:569–582.

Carlson L, Schwertmann U. 1990. The effect of CO_2 and oxidation rate on the formation of goethite versus lepidocrocite from an Fe(II) system at pH 6 and 7. Clay Miner 25:65–71.

Chapman BM, Jones DR, Jung RF. 1983. Processes controlling metal ion attenuation in acid mine drainage streams. Geochim Cosmochim Acta 47:1957–1973.

Dutrizac JE, Kaiman S. 1976. Synthesis and properties of jarosite-type compounds. Can Mineral 14:151–158.

Ficklin WH, Love AH, Papp CSE. 1991. Solid-phase variations in an aquifer as the aqueous solution changes, Globe, Arizona. In: Mallard GE, Aronson DA, editors. USGS toxic substances hydrology program, Proc Tech Meet. Water-resources investigations report 91-4034. p 475–480.

Filipek LH, Nordstrom DK, Ficklin WH. 1987. Interaction of acid mine drainage with waters and sediments of West Squaw Creek in the West Shasta Mining district, California. Environ Sci Technol 21:388–396.

Goldman DS. 1979. A reevaluation of the Mössbauer spectroscopy of calcic amphiboles. Am Mineral 64:109–118.

Herbert RB. 1994. Metal transport in groundwater contaminated by acid mine drainage. Nordic Hydrol 25:193–212.

Herbert RB. 1995a. Precipitation of Fe oxydroxides and jarosite from acidic groundwater. GFF 117:81–85.

Herbert RB. 1995b. The geochemistry of groundwater and soils contaminated by acid mine leachate: A field study from Rudolfsgruvan, Dalarna, Sweden [Ph.D. thesis]. Uppsala, Sweden: Institution of Earth Sciences, Uppsala Univ. 133 p.

Herbert RB. 1996. Metal retention by iron oxide precipitation from acid ground water in Dalarna, Sweden. Applied Geochem 11:229–236.

Jambor JL. 1994. Mineralogy of sulfide-rich tailings and their oxidation products. In: Jambor J, Blowes D, editors. Handbook on environmental geochemistry of sulfide minewastes. Mineral Assoc Can 22:59–102.

JCPDS, Joint Committee on Powder Diffraction Standards. 1972. Selected powder diffraction data for minerals. Publication DBM-1-23. Swarthmore, PA: JCPDS.

Johnson CA. 1986. The regulation of trace element concentrations in river and estuarine waters contaminated with acid mine drainage: The adsorption of Cu and Zn on amorphous Fe oxyhydroxides. Geochim Cosmochim Acta 50: 2433–2438.

Karlsson S, Allard B, Håkansson K. 1988. Chemical characterization of stream-bed sediments receiving high loadings of acid mine effluents. Chem Geol 67:1–15.

Klug HP, Alexander LE. 1974. X-ray diffraction procedures for polycrystalline and amorphous materials. New York: J Wiley. 966 p.

Langmuir D, Whittemore DO. 1971. Variations in the stability of precipitated ferric oxyhydroxides. In: Gould RF, editor. Nonequilibrium systems in natural water chemistry. Adv Chem Ser 106:209–234.

Leclerc A. 1980. Room temperature Mössbauer analysis of jarosite-type compounds. Phys Chem Miner 6:327–334.

Murad E. 1982. The characterization of goethite by Mössbauer spectroscopy. Am Mineral 67:1007–1011.

Murad E. 1988. Properties and behavior of iron oxides as determined by Mössbauer spectroscopy. In: Stucki JW,

Goodman BA, Schwertmann U, editors. Iron in soils and clay minerals. Dordrecht: D. Reidel. p 309–350.

Murad E, Bigham JM, Bowen LH, Schwertmann U. 1990. Magnetic properties of iron oxides produced by bacterial oxidation of Fe^{2+} under acid conditions. Hyperfine Interact 58:2373–2376.

Murad E, Schwertmann U. 1980. The Mössbauer spectrum of ferrihydrite and its relations to those of other iron oxides. Am Mineral 65:1044–1049.

Nordstrom DK. 1982. Aqueous pyrite oxidation and the consequent formation of secondary iron minerals. In: Hossner LR, editor. Acid sulfate weathering. SSSA publication 10. Madison: Soil Sci Soc Am. p 95–108.

Postma D. 1993. The reactivity of iron oxides in sediments: A kinetic approach. Geochim Cosmochim Acta 57:5027–5034.

Ripmeester JA, Ratcliffe CI, Dutrizac JE, Jambor JL. 1986. Hydronium ion in the alunite-jarosite group. Can Mineral 24:435–447.

Schulze DG. 1981. Identification of soil iron oxide minerals by differential X-ray diffraction. Soil Sci Soc Am J 45: 437–440.

Schulze DG. 1984. The influence of aluminum on iron oxides. VIII. Unit-cell dimensions of Al-substituted goethites and estimation of Al from them. Clays Clay Miner 32:36–44.

Schulze DG, Schwertmann U. 1984. The influence of aluminum on iron oxides. X. Properties of Al-substituted goethites. Clay Miner 19:521–539.

Schwertmann U. 1964. Differenzierung der Eisenoxides des Bodens durch photochemische Extraktion mit saurer Ammoniumoxalat-Lösung. Z Pflanzenernähr Bodenkd 105: 194–202.

Schwertmann U. 1973. Use of oxalate for Fe extraction from soils. Can J Soil Sci 53:244–246.

Schwertmann U. 1985. The effect of pedogenic environments on iron oxide minerals. Adv Soil Sci 1:172–200.

Schwertmann U, Cambier P, Murad E. 1985. Properties of goethites of varying crystallinity. Clays Clay Miner 33: 369–378.

Schwertmann U, Carlson L. 1994. Aluminum influence on iron oxides: XVII. Unit-cell parameters and aluminum substitution on natural goethites. Soil Sci Soc Am J 58:256–261.

Schwertmann U, Carlson L, Murad E. 1987. Properties of iron oxides in two Finnish lakes in relation to the environment of their formation. Clays Clay Miner 35:297–304.

Schwertmann U, Cornell RM. 1991. Iron oxides in the laboratory: Preparation and characterization. Weinheim: VCH Verlagsgesellschaft mbH. 137 p.

Schwertmann U, Taylor RM. 1989. Iron oxides. In: Dixon JB, Weed SB, editors. Minerals in soil environments, 2nd ed. Madison, WI: Soil Sci Soc Am. p 379–438.

Stollenwerk K. 1994. Geochemical interactions between constituents in acidic groundwater and alluvium in an aquifer near Globe, Arizona. Applied Geochem 9:353–369.

Ribet I, Ptacek CJ, Blowes DW, Jambor JL. 1995. The potential for metal release by reductive dissolution of weathered mine tailings. J Contam Hydrol 17:239–273.

WaveMetrics. 1994. Igor Pro user's manual 2.00. Lake Oswego, OR: WaveMetrics Inc. 1080 p.

(Received 29 June 1995; accepted 24 May 1996; Ms. 2662)